Neurobiology of Disease

Spinocerebellar Ataxia Type 7 Cerebellar Disease Requires the Coordinated Action of Mutant Ataxin-7 in Neurons and Glia, and Displays Non-Cell-Autonomous Bergmann Glia Degeneration

Stephanie A. Furrer,[1] **Mathini S. Mohanachandran,**[1] **Sarah M. Waldherr,**[1] **Christopher Chang,**[1] **Vincent A. Damian,**[2] **Bryce L. Sopher,**[1] **Gwenn A. Garden,**[1,4] **and Albert R. La Spada**[3,5,6]

Departments of [1]Neurology, [2]Biochemistry, and [3]Medicine (Medical Genetics), and [4]The Center on Human Development and Disability, University of Washington, Seattle, Washington 98195, and [5]Departments of Pediatrics, Cellular and Molecular Medicine, and Neurosciences, Division of Biological Sciences, and the Institute for Genomic Medicine, University of California, San Diego, La Jolla, California 92093, and [6]Rady Children's Hospital, San Diego, California 92123

Spinocerebellar ataxia type 7 (SCA7) is a dominantly inherited disorder characterized by cerebellum and brainstem neurodegeneration. SCA7 is caused by a CAG/polyglutamine (polyQ) repeat expansion in the ataxin-7 gene. We previously reported that directed expression of polyQ-ataxin-7 in Bergmann glia (BG) in transgenic mice leads to ataxia and non-cell-autonomous Purkinje cell (PC) degeneration. To further define the cellular basis of SCA7, we derived a conditional inactivation mouse model by inserting a loxP-flanked ataxin-7 cDNA with 92 repeats into the translational start site of the murine prion protein (PrP) gene in a bacterial artificial chromosome (BAC). The *PrP-floxed-SCA7-92Q BAC* mice developed neurological disease, and exhibited cerebellar degeneration and BG process loss. To inactivate polyQ-ataxin-7 expression in specific cerebellar cell types, we crossed *PrP-floxed-SCA7-92Q BAC* mice with *Gfa2-Cre* transgenic mice (to direct Cre to BG) or *Pcp2-Cre* transgenic mice (which yields Cre in PCs and inferior olive). Excision of ataxin-7 from BG partially rescued the behavioral phenotype, but did not prevent BG process loss or molecular layer thinning, while excision of ataxin-7 from PCs and inferior olive provided significantly greater rescue and prevented both pathological changes, revealing a non-cell-autonomous basis for BG pathology. When we prevented expression of mutant ataxin-7 in BG, PCs, and inferior olive by deriving *Gfa2-Cre;Pcp2-Cre;PrP-floxed-SCA7-92Q BAC* triple transgenic mice, we noted a dramatic improvement in SCA7 disease phenotypes. These findings indicate that SCA7 disease pathogenesis involves a convergence of alterations in a variety of different cell types to fully recapitulate the cerebellar degeneration.

Introduction

Spinocerebellar ataxia type 7 (SCA7) is a progressive, dominantly inherited neurodegenerative disorder characterized by neuron dysfunction, culminating in cell loss in the retina, cerebellum, and brainstem. SCA7 patients consequently exhibit ataxia, motor system abnormalities, blindness, and early mortality. SCA7 is caused by a CAG/polyglutamine (polyQ) repeat expansion in the coding region of the ataxin-7 gene. As in other diseases caused by polyQ repeat expansion, ataxin-7 is ubiquitously expressed. Nonetheless, inheriting polyQ-expanded ataxin-7 yields degeneration in specific neuronal populations that are selectively vulnerable to this mutation (Garden and La Spada, 2008).

A number of mouse models have been generated to investigate SCA7 disease pathogenesis. PolyQ-expanded ataxin-7, expressed in cerebellar Purkinje cells (PCs) using the Pcp2 promoter, produced very mild ataxia with no impact on life span (Yvert et al., 2000). Using the murine prion protein (PrP) transgenic expression system, we expressed polyQ-expanded ataxin-7 throughout the CNS, but not in PCs. The resulting *PrP-SCA7-c92Q* mice developed ataxia and PC degeneration, documenting a role for non-cell-autonomous PC degeneration in SCA7 disease pathogenesis (Garden et al., 2002). Transgenic mice that express ataxin-7-92Q protein only in Bergmann glia (BG) in the cerebellum also develop ataxia and PC degeneration, implicating glial dysfunction in polyQ-ataxin-7-mediated PC degeneration (Custer et al., 2006).

While these studies underscored the importance of specific non-neuronal cell types in cerebellar degeneration, PCs are integrated into a complex neural network and receive glutamatergic

input from axons projecting from the inferior olive (IO) and cerebellar granule cells. BG remove excess glutamate from PC synapses (Huang and Bordey, 2004) and secrete neurotrophic factors, which support PCs (Mount et al., 1995). IO neurons produce insulin-like growth factor 1, a neurotrophic factor that promotes PC survival and glutamate-aspartate transporter (GLAST) expression in BG (Nieto-Bona et al., 1993; Gamboa and Ortega, 2002).

To clarify the cellular basis of SCA7, we developed a powerful new mouse model wherein polyQ-ataxin-7 expression could be spatially and temporally regulated. In this model, an ataxin-7 92Q cDNA is flanked by loxP sites at the start site of translation in the murine PrP gene in a bacterial artificial chromosome (BAC). The *PrP-floxed-SCA7-92Q BAC* mice ubiquitously express mutant ataxin-7 protein in all neurons, including PCs, and develop cerebellar ataxia and histopathology. To determine which cell types are required for SCA7 disease pathogenesis, *PrP-floxed-SCA7-92Q BAC* mice were crossed with driver lines expressing Cre-recombinase in BG (*Gfa2-Cre*) or in PCs and IO (*Pcp2-Cre*). *Gfa2-Cre;PrP-floxed-SCA7-92Q BAC* and *Pcp2-Cre;PrP-floxed-SCA7-92Q BAC* bigenic mice each displayed a less severe phenotype than *PrP-floxed-SCA7-92Q BAC* littermates. Excision of ataxin-7-92Q from PCs and IO neurons not only protected against cerebellar atrophy, but also prevented BG pathology. Excision of ataxin-7-92Q from BG, however, did not prevent these pathological features, suggesting that BG pathology is non-cell autonomous in SCA7. When we created triple transgenic (i.e., *Gfa2-Cre; Pcp2-Cre; PrP-floxed-SCA7-92Q BAC*) mice, onset of cerebellar ataxia was delayed up to 20 weeks. Together, these findings indicate that BG, PCs, and IO neurons interact in an intimate and tightly interconnected network, and, thus, together contribute to SCA7.

Materials and Methods

Generation of PrP-floxed-SCA7-92Q BAC mice
We obtained a 90 kb fragment containing the murine PrP in a BAC vector backbone (RPCI mouse BAC library 24; clone ID RP24–92I12). The murine PrP BAC targeting vector was performed in five steps, as follows: (1) 5′ and 3′ targeting arms were inserted by PCR onto the ends of a minimal 1.8 kb, chloramphenicol-resistant vector; (2) an ampicillin resistance cassette was cloned into the MluI, XmaI sites of the targeting vector; (3) a 234 bp fragment encoding the last 50 aa of ataxin-7, followed by a loxP site, was inserted into the XhoI, HpaI restriction sites of the targeting vector; (4) an 824 bp fragment encoding a 3× FLAG tag fused to EGFP was cloned into the NheI, PacI restriction sites of the targeting vector; and (5) a 2.8 kb fragment containing a loxP site, followed by the remaining ataxin-7-92Q sequence, was cloned into the MluI, XhoI restriction sites to complete the targeting vector. The targeting vector was recombined into the BAC vector backbone and replaced all coding information for the murine PrP gene. The final PrP-floxed-SCA7-92Q BAC vector was microinjected into C57BL/6J:C3H/HeJ F1 hybrid oocytes. Of four founders identified, two gave rise to *PrP-floxed-SCA7-92Q BAC* lines with comparable phenotypes. Of these lines, we chose to focus our studies principally on line 258′.

PCR genotyping
Mice tissue (~2–4 mm²) was placed in a 1.5 ml Microfuge tube containing 175 μl of 0.1 M NaOH and 175 μl of mineral oil. Tubes were briefly centrifuged and then heated in an Oster Food Steamer (Target) for 45 min. The tubes were removed from the steamer, inverted several times, and then centrifuged at 13,000 × g in a benchtop centrifuge for 3 min. Eighty microliters of base solution was carefully taken from the middle of the aqueous phase. This material was transferred to a new 0.65 ml Microfuge tube containing 80 μl of 1 M Tris-HCl. This neutralized tissue extract was stored at 4°C before PCR analysis. PCR conditions included 60°C annealing temperature, 38 cycles, and 1 min extension period. Primer sequences are shown in Table 1.

Table 1. Primer sequences

Transgene	Primer sequence	Product (bp)
PrP-floxed-SCA7-92Q BAC		
Forward	CATTTTAGGCCCCACGTATCAC	587
Reverse	GGCCCGCTCCGACAT	
CMV-Cre		
Forward	CAAAATTTGCCTGCATTACCG	553
Reverse	CATTCTCCCACCGTCAGTACG	
Z/EG		
Forward	GACGACGGCAACTACAAGACC	561
Reverse	GCCAGAAGTCAGATGCTCAAG	
Gfa2-Cre		
Forward	GTGCTGGGATTACAAGCATGA	400
Reverse	CAGGCAAATTTTGGTGTACGG	
Pcp2-Cre		
Forward	GATGGATTTCCGTCTCTGGTG	428
Reverse	CATTATAAGCTGCAATAAACAAGTTCTGC	

RT-PCR analysis
Mouse brains were homogenized in Trizol (Life Technologies), and total RNA was extracted according to the manufacturer's instructions. Total RNA was reverse transcribed in independent duplicate reactions using random hexamers and SuperScript II reverse transcriptase (Life Technologies), and quantification of mouse and human ataxin-7 RNA expression by coamplification and subsequent restriction digestion was performed as previously described (La Spada et al., 2001). Total RNA was isolated from the cerebellum of 6-week-old mice using an RNeasy isolation kit (Qiagen). Total RNA was reverse transcribed using SuperScriptII Reverse Transcriptase according to manufacturer's instructions (Invitrogen). The cDNAs were subjected to real-time PCR using custom ataxin-7 primers and probe selected with Primer Express v3.0 software (Applied Biosystems), as follows: forward primer, TTTGGGAGCCGGCAGAT; reverse primer, GCTGTGCATTCAGATGCTTCTC; probe, TGTTT-GACTCCAGGTGGA. Samples were analyzed on a StepOnePlus Real-Time PCR system using a 64°C annealing temperature and normalized to mouse 18S RNA using Applied Biosystems assay Hs99999901_s1. Average ataxin-7 RNA level for nontransgenic and *PrP-floxed-SCA7-92Q BAC* mice ($n \geq 3$/group) was calculated using Microsoft Excel. Ataxin-7 levels in nontransgenic animals was normalized to 1.0, and data were plotted and statistically analyzed in Graphpad Prism 4.0.
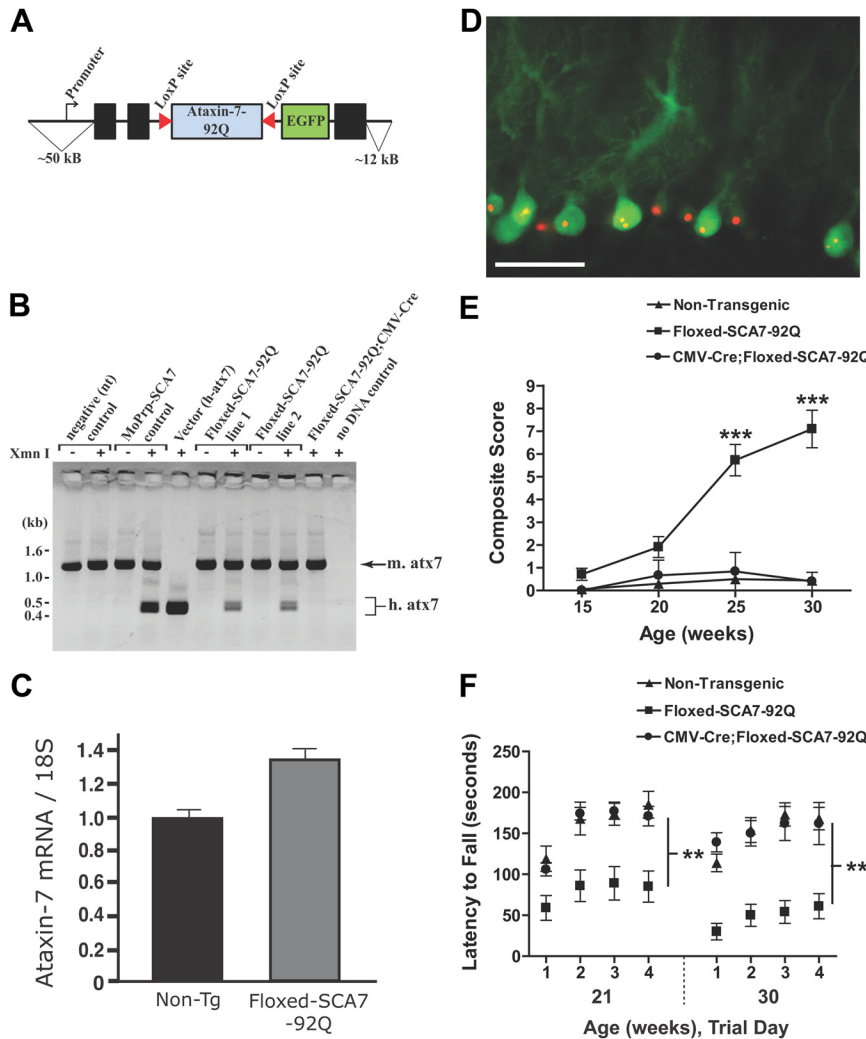
Behavioral phenotyping
All studies and procedures were approved by the University of Washington and University of California, San Diego, Institutional Animal Care and Use Committees (IACUC). Females and males were used in all studies, and experiments were performed by a blinded examiner.

Composite phenotype score. The composite phenotype score was performed as previously described (Guyenet et al., 2010). An average composite phenotype score for each genotype was calculated and plotted using Microsoft Excel. Statistical analyses were conducted in Graphpad Prism 4.0.

Accelerating rotarod. Mice were placed on the rotarod (Economex, Columbia Instruments) and trained on day 0 by running freely up to 5 min. On days 1–4, mice were placed on the rotarod and underwent the following regimen: at time 0, the rotarod was started with four rotations per minute, and an acceleration of 0.1 rotations per second. The time each mouse dismounted was recorded (in seconds), and mice had at least 5 min of rest between trials. Trials were repeated five times daily for a maximum of 300 s per trial. The best four times per day were recorded and averaged for each mouse. Average latency to fall for each trial day was calculated for each genotype and plotted using Microsoft Excel. Statistical analyses were conducted in Graphpad Prism 4.0.

Immunohistochemistry
Deeply anesthetized mice were transcardially perfused with PBS followed by 4.0% paraformaldehyde (PFA) in 0.1 M phosphate buffer (PB), pH 7.4. Brains were removed and postfixed in 4.0% PFA in 0.1 M PB overnight, then moved into 0.4% PFA in 0.1 M PB for storage at 4°C. Free-floating 40 μm sagittal brain sections were cut on the Leica Vibratome 1000S and

anti-mouse IgG (Invitrogen) at 1:500 dilution were applied to sections and incubated at room temperature for 2–3 h. After three washes in 1× PBS, sections were mounted on glass slides and coverslipped in Fluoro-Gel with Tris Buffer (Electron Microscopy Sciences). Sections were viewed and 2-D or 3-D z-stack digital images were created using a Zeiss Axiovert 200M inverted microscope and Slidebook 5.0 software (Intelligent Imaging Innovations).

To quantify *PrP-floxed-SCA7-92Q BAC* gene excision, 2-D images were collected from three areas per section, one section per animal, for *Gfa2-Cre;Z/EG* and *Z/EG* animals (*n* = 6/group). 2-D images were collected of four areas per section, one section per animal, for *Pcp2-Cre;PrP-floxed-SCA7-92Q BAC* (*n* = 7) and *PrP-floxed-SCA7-92Q BAC* (*n* = 4) mice. Two independent observers counted the number of either calbindin-positive Purkinje cells or S-100β-positive Bergmann glia, then counted the number of those that were GFP positive. Results were reported as a ratio of GFP and marker double-positive cells to total marker-positive cells. Average ratios for each genotype were calculated, plotted, and analyzed statistically in Graphpad Prism 4.0.

To quantify cerebellar molecular layer thickness, 2-D images of calbindin-immunostained cerebellar sections were collected. The three most dorsal cerebellar folia per section, using three sections per individual (*n* = 6/group), were imaged. In each image, a boundary line around the molecular layer from, but excluding, the Purkinje cell bodies to the pial surface was drawn by hand using Slidebook 5.0. In the center of the molecular layer, 100-μm-long lines were drawn. Every 100 μm, a measurement was taken from the pial surface to the Purkinje cell layer. Molecular layer measurements were averaged for each genotype, plotted, and analyzed statistically in Graphpad Prism 4.0.

To quantify the number of Bergmann glia processes, brightest-point projection images were created using Slidebook 5.0. 3-D image z-stacks were collected for two areas per section, three sections per individual (*n* = 6/group). 3-D images were deconvolved using the Nearest Neighbors algorithm of Slidebook 5.0. The brightest-point projection images were created through the z-axis to produce 2-D images. In each 2-D image, a 150 μm line was drawn using Slidebook 5.0 (Intelligent Imaging Innovations) ~50 μm from the pial surface of the cerebellar molecular layer. Three independent observers drew this line and then counted the number of GFAP-positive processes that crossed the line. The average number of processes for each genotype was calculated, plotted, and analyzed statistically in Graphpad Prism 4.0.

Figure 1. *PrP-floxed-SCA7-92Q BAC mice exhibit Cre-dependent ataxin-7 expression and disease phenotype. **A**, Diagram of the PrP-floxed-SCA7-92Q BAC construct, indicating the location of the human ataxin-7 92Q cDNA flanked by loxP sites, a downstream EGFP reporter gene, and the first two exons and last exon from the murine prion protein gene (black boxes; not to scale). **B**, We performed RT-PCR analysis of cerebella with primers that coamplified murine and human ataxin-7, and then differentiated mouse endogenous ataxin-7 (m. atx7) from human transgenic ataxin-7 (h. atx7) by XmnI restriction digestion. PrP-floxed-SCA7-92Q transgene-positive mice yielded XmnI-cut bands, which were no longer present after crossing with CMV-Cre mice that ubiquitously express Cre recombinase. **C**, We performed quantitative RT-PCR analysis of cerebellar RNA with primers that coamplified murine and human ataxin-7, normalized to mouse 18S RNA levels, for nontransgenic and PrP-floxed-SCA7-92Q BAC mice (n = 3/group). We set the total ataxin-7 level to 1 in the nontransgenic control and found that the total ataxin-7 level in the PrP-floxed-SCA7-92Q BAC mice is ~1.3, indicating that the BAC transgene is expressed at lower than endogenous levels. **D**, Immunofluorescent labeling of ataxin-7 (red) and calbindin (green) in cerebellar sections from 40-week-old PrP-floxed-SCA7-92Q BAC mice. Scale bar, 50 μm. **E**, We completed composite phenotype analysis for sets of nontransgenic (n = 14), PrP-floxed-SCA7-92Q BAC (n = 10), and CMV-Cre;Floxed-SCA7-92Q BAC (n = 5) mice. PrP-floxed-SCA7-92Q BAC mice develop a significant phenotype, which is eliminated upon Cre-mediated excision (***p < 0.001, two-way ANOVA with Bonferroni's post hoc test). Error bars indicate SEM. **F**, We measured the mean latency to fall from the accelerating rotarod for sets of nontransgenic (n = 10), PrP-floxed-SCA7-92Q BAC (n = 10), and CMV-Cre;PrP-floxed-SCA7-92Q BAC (n = 5) mice. PrP-floxed-SCA7-92Q BAC mice performed significantly worse on the rotarod at 21 and 30 weeks of age compared with nontransgenics, and CMV-Cre;PrP-floxed-SCA7-92Q BAC mice performed much better than PrP-floxed-SCA7-92Q BAC mice at these time points (**p < 0.01, two-way ANOVA with Bonferroni's post hoc test). Error bars indicate SEM.*

stored in 0.03% PFA in PBS. Free-floating sections were incubated with 5% normal goat serum (NGS), 0.2% BSA, and 1.0% Triton X-100 for 1 h at room temperature. Sections were then incubated overnight at 4°C with anti-calbindin antibody (300, Swant) at 1:1000 dilution; anti-GFP antibody (ab6556, Abcam) at 1:1000 dilution; anti-GFAP antibody (Z0334, DAKO) at 1:1000 dilution; anti-S100β antibody (ab11178, Abcam) at 1:1000 dilution; or anti-ataxin-7 antibody (PA1-749, Affinity Bioreagents) at 1:500 dilution in PBS with 5% NGS and 0.1% Triton X-100. After three washes in 1× PBS, AlexaFluor 488 anti-rabbit or anti-mouse IgG (Invitrogen) at 1:500 dilution, and/or AlexaFluor 594 anti-rabbit or

Results

Characterization of the *PrP-floxed-SCA7-92Q BAC* transgenic mouse

To generate a mouse model that can delineate cell type-specific contributions to SCA7 disease pathogenesis, we inserted an ataxin-7 cDNA, carrying 92 CAG repeats and flanked by loxP sites, into a murine prion protein BAC, and placed an EGFP reporter gene
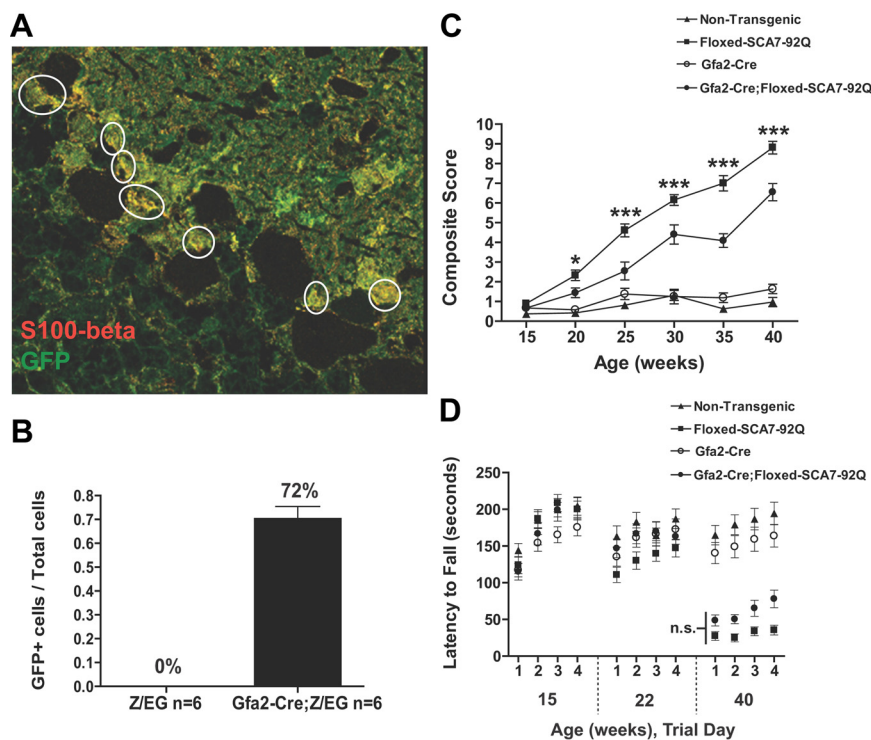
downstream of the ataxin-7 cDNA (Fig. 1*A*). After transgenic microinjection of this BAC construct, we identified founders and established two independent *PrP-floxed-SCA7-92Q BAC* lines. RT-PCR analysis of cerebellar RNA from *PrP-floxed-SCA7-92Q BAC* mice demonstrated that both *PrP-floxed-SCA7–92Q BAC* lines expressed human ataxin-7 (Fig. 1*B*). Quantitative real-time RT-PCR analysis of ataxin-7 on RNA extracted from cerebellum confirmed that transgene expression was less than endogenous ataxin-7 expression (Fig. 1*C*). To ensure Cre recombinase-mediated excision of the ataxin-7 cDNA, we crossed *PrP-floxed-SCA7-92Q BAC* mice with *CMV-Cre* transgenic mice. The resulting *CMV-Cre; PrP-floxed-SCA7-92Q BAC* bigenic mice no longer expressed human ataxin-7, confirming successful Cre-mediated bigenic mice no longer expressed human excision (Fig. 1*B*). Immunofluorescent labeling of *PrP-floxed-SCA7-92Q BAC* brain sections with an anti-ataxin-7 antibody revealed widespread expression of the mutant protein, as evidenced by aggregate formation in neurons, including granule cell neurons (GCNs) and Purkinje cell neurons (Fig. 1*D*). *PrP-floxed-SCA7-92Q BAC* mice did not exhibit a significant reduction in calbindin-labeled PC soma (2.6 ± 0.1 PCs per 100 μm; ±SEM) compared with nontransgenic mice (3.0 ± 0.2 PCs per 100 μm; ±SEM) (p =0.13, unpaired two-tailed t test), similar to previously published mouse models of SCA7 (Garden et al., 2002; Chou et al., 2010).

Figure 2. Excision of polyQ-ataxin-7 from Bergmann glia partially ameliorates SCA7 neurological phenotypes. *A*, Immunofluorescence labeling of EGFP (green) and S100-β (red) in *Gfa2-Cre;Z/EG* cerebellar sections. *B*, Gfa2-Cre expression produced a 72% excision rate in Bergmann glia. *C*, We performed composite phenotype analysis for sets of nontransgenic ($n = 16$), *PrP-floxed-SCA7-92Q* ($n = 13$), *Gfa2-Cre* ($n = 14$), and *Gfa2-Cre;PrP-floxed-SCA7-92Q BAC* ($n = 11$) mice. Excision of polyQ-ataxin-7 from Bergmann glia in *Gfa2-Cre;PrP-floxed-SCA7-92Q BAC* mice yielded a markedly improved composite phenotype compared with *PrP-floxed-SCA7-92Q BAC* mice beginning at 20 weeks of age (*$p < 0.05$, ***$p < 0.001$, two-way ANOVA with Bonferroni's *post hoc* test). Error bars indicate SEM. *D*, When we analyzed these cohorts by accelerating rotarod testing, we found that *PrP-floxed-SCA7-92Q BAC* mice perform significantly worse than nontransgenic and *Gfa2-Cre* mice at 40 weeks of age ($p < 0.001$, two-way ANOVA with Bonferroni's *post hoc* test). *Gfa2-Cre;PrP-floxed-SCA7-92Q BAC* mice exhibited a trend toward improved rotarod performance, but this was not significant. Error bars indicate SEM.

Motor behavior in *PrP-floxed-SCA7-92Q BAC* mice was assessed using a composite phenotype scoring system (Guyenet et al., 2010) and by rotarod analysis. Beginning at 20 weeks of age, *PrP-floxed-SCA7-92Q BAC* mice exhibited a more severe behavioral phenotype than nontransgenic mice, based upon composite phenotype score, and this progressively worsened with age (Fig. 1*E*). *PrP-floxed-SCA7-92Q BAC* mice also performed significantly worse on the accelerating rotarod at 21 weeks of age compared with nontransgenic littermates, and their rotarod performance worsened at 30 weeks of age (Fig. 1*F*). CMV-Cre-driven excision of the ataxin-7 cDNA prevented these phenotypes in *CMV-Cre;PrP-floxed-SCA7-92Q BAC* bigenic mice, as these bigenic mice performed comparably to nontransgenic mice (Fig. 1*E,F*). Together, these results indicate that the *PrP-floxed-SCA7-92Q BAC* transgenic mice develop a SCA7 phenotype characterized by progressive ataxia and impaired motor function. Furthermore, the utility of this model for studying cell-type contribution was confirmed by widespread Cre-mediated excision of the mutant ataxin-7 gene.

**PolyQ-ataxin-7 expression in Bergmann glia is required for the full SCA7 phenotype**
We have previously shown that expression of polyQ-expanded ataxin-7 in BG, driven by a human glial fibrillary acidic protein promoter known as Gfa2′ (Besnard et al., 1991), is sufficient to produce SCA7 cerebellar neurodegeneration (Custer et al., 2006). To determine whether mutant ataxin-7 expression in BG is re-

quired for the full SCA7 phenotype, we crossed a mouse line expressing Cre recombinase driven by the Gfa2 promoter (Zhuo et al., 2001) with the *PrP-floxed-SCA7-92Q BAC* mice. In *PrP-floxed-SCA7-92Q BAC* mice, EGFP expression is induced upon Cre-mediated excision of the loxP flanked ataxin-7 cDNA, as EGFP is moved adjacent to the murine prion protein promoter. In *Gfa2-Cre;PrP-floxed-SCA7-92Q BAC* mice, EGFP expression is low and BG cell bodies are very compact, complicating determination of the excision rate in bigenic BG. Thus, to validate this driver line, we crossed *Gfa2-Cre* mice with a robust Z/EG reporter line (Novak et al., 2000). Sagittal brain sections from *Gfa2-Cre; Z/EG* mice were immunolabeled for GFP and S100-β, a BG cell body marker. We found that 72% of all S100-β-positive BG were concurrently positive for GFP (Fig. 2*A,B*), validating the utility of the Gfa2-Cre driver line for high-level BG excision.

We assessed the behavioral phenotype of *Gfa2-Cre;PrP-floxed-SCA7–92Q BAC* bigenic mice by again using the composite phenotype score and accelerating rotarod. As expected, *PrP-floxed-SCA7-92Q BAC* mice displayed significantly higher composite phenotype scores, beginning at 20 weeks of age (Fig. 2*C*). *Gfa2-Cre;PrP-floxed-SCA7-92Q BAC* mice, however, displayed a progressive, but less severe phenotype compared with *PrP-floxed-SCA7-92Q BAC* littermates. On the accelerating rotarod, *PrP-floxed-SCA7-92Q BAC* mice performed poorly at 22 weeks of age and were significantly impaired by 40 weeks of age (Fig. 2*D*). *Gfa2-Cre;PrP-floxed-SCA7-92Q BAC* mice performed poorly on
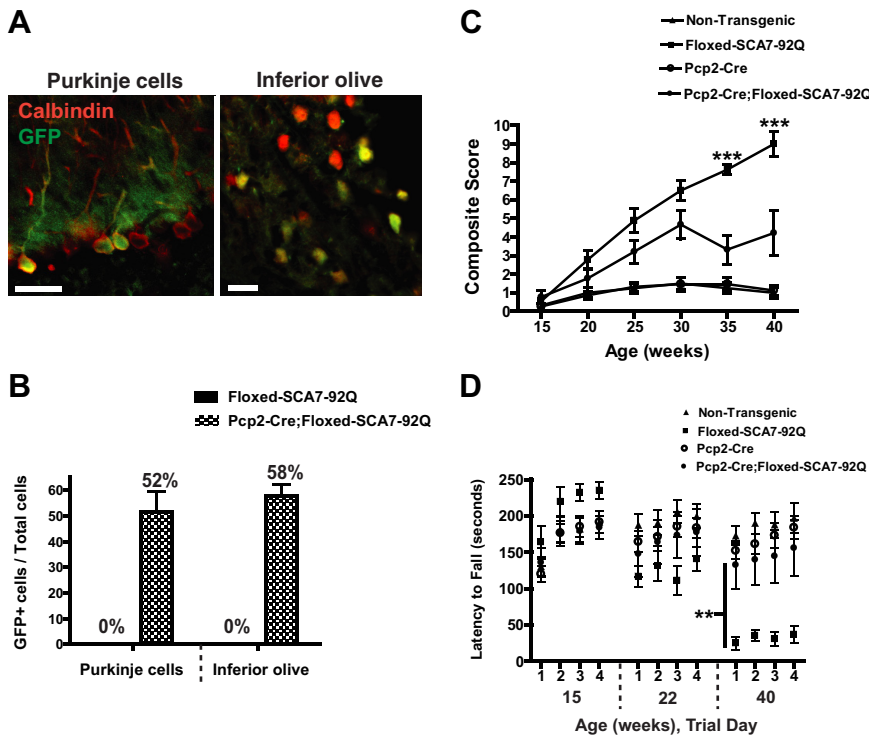
Figure 3. Excision of polyQ-ataxin-7 from Purkinje cells and inferior olive partially ameliorates SCA7 neurological phenotypes. *A*, Immunofluorescence labeling of EGFP (green) and calbindin (red) in *Pcp2-Cre;PrP-floxed-SCA7-92Q BAC* bigenic cerebellum and brainstem sections. Scale bars, 50 μm. *B*, Pcp2-driven Cre expression yielded a 52% excision rate in Purkinje cells and a 58% excision rate in inferior olive neurons. *C*, Composite phenotyping revealed that *Pcp2-Cre;PrP-floxed-SCA7-92Q BAC* mice (*n* = 9) are moderately improved compared with *PrP-floxed-SCA7-92Q BAC* mice (*n* = 8) from 20 to 30 weeks of age, but not compared with nontransgenic (*n* = 12) or *Pcp2-Cre* (*n* = 15) controls. Moreover, the neurological phenotype of *Pcp2-Cre;PrP-floxed-SCA7-92Q BAC* mice ceases to progress after 30 weeks of age, and thus becomes dramatically improved compared with their progressing *PrP-floxed-SCA7-92Q BAC* littermates at these time points (***p < 0.001, two-way ANOVA with Bonferroni's *post hoc* test). Error bars indicate SEM. *D*, *Pcp2-Cre;PrP-floxed-SCA7-92Q BAC* mice exhibit a trend toward improved rotarod performance at 22 weeks of age. By 40 weeks of age, however, *Pcp2-Cre;PrP-floxed-SCA7-92Q BAC* mice are markedly superior to their *PrP-floxed-SCA7-92Q BAC* littermates, and actually perform comparably to nontransgenic and Pcp2-Cre controls on the accelerating rotarod (**p < 0.01, two-way ANOVA with Bonferroni's *post hoc* test). Error bars indicate SEM.

mented that expression of Cre in this line is not limited to PCs, but is also present in the inferior olive, the superior olive, and the olfactory bulb (Fig. 3A; data not shown). These studies thus reconfirmed the integrity of the *PrP-floxed-SCA7–92Q BAC* construct, as singly transgenic *PrP-floxed-SCA7-92Q* cerebellar sections showed no EGFP immunoreactivity, indicating that EGFP expression is only released upon Cre-mediated gene excision (Fig. 3B).

Neurons of the IO degenerate in SCA7 patients (Garden and La Spada, 2008) as well as in SCA7 transgenic mice (Wang et al., 2010). The IO projects climbing fibers (CFs) that form glutamatergic synapses on PC somae and dendrites. The IO also delivers the neurotrophic factor insulin-like growth factor-1 (IGF-1) to PCs (Nieto-Bona et al., 1993). Thus, loss of climbing fiber input to PCs may contribute to non-cell-autonomous PC degeneration in SCA7. When we quantified the percentage of calbindin-positive IO neurons that also express GFP to determine excision rate, as was just described for PCs, we found that ataxin-7 cDNA excision had occurred in 58% of IO neurons (Fig. 3A,B). Composite phenotype scoring indicated that *Pcp2-Cre;PrP-floxed-SCA7-92Q BAC* bigenic mice had a significantly milder phenotype than their singly transgenic SCA7 littermates, and, interestingly, neurological impairment in *Pcp2-Cre;PrP-floxed-SCA7-92Q BAC* mice reached a plateau at 30 weeks of age (Fig. 3C). Accelerating rotarod analysis at 22 weeks of age indicated that *PrP-floxed-SCA7-92Q BAC* mice displayed evidence of motor incoordination at this time, while

Pcp2-Cre;PrP-floxed-SCA7-92Q BAC bigenic mice performed comparably to nontransgenic and Pcp2-Cre controls (Fig. 3D). By 40 weeks of age, the motor performance differences became quite dramatic, as *Pcp2-Cre;PrP-floxed-SCA7-92Q BAC* bigenic mice remained on the rotarod at least four times longer than their *PrP-floxed-SCA7-92Q BAC* littermates. Together, these findings demonstrate that expression of mutant ataxin-7 in IO neurons, and likely also in PCs, is required to recapitulate the full SCA7 phenotype.

PolyQ-ataxin-7 excision in Purkinje cells and inferior olive, but not in Bergmann glia, protects against cerebellar molecular layer degeneration
A prominent feature of SCA7 neurodegeneration in transgenic mice is shortened PC dendritic arbors in the cerebellar molecular layer (Garden et al., 2002; Yoo et al., 2003; Custer et al., 2006; Chou et al., 2010). To investigate whether this loss is mitigated in *Gfa2-Cre;PrP-floxed-SCA7-92Q BAC* or *Pcp2-Cre;PrP-floxed-SCA7-92Q BAC* bigenic mice, we immunostained sagittal cerebellar sections with anti-calbindin antibody. By 40 weeks of age, we noted reduced dendritic calbindin immunoreactivity, abnormal PC morphology, and molecular layer thinning in the cerebellum of *PrP-floxed-SCA7-92Q BAC* mice (Fig. 4A,B). *Gfa2-Cre;PrP-floxed-SCA7-92Q BAC* bigenic mice also exhibited reduced calbindin immunoreactivity and a thinner molecular layer, similar to

the accelerating rotarod at 40 weeks as well, but tended to remain on the rotarod longer than their *PrP-floxed-SCA7-92Q BAC* littermates (Fig. 2D). Together, these data suggest that polyQ-expanded ataxin-7 expression in BG contributes to SCA7 pathogenesis and is required to recapitulate the full SCA7 behavioral phenotype.

PolyQ-ataxin-7 expression in inferior olive is required for SCA7 disease phenotype
Restricted expression of polyQ-expanded ataxin-7 in cerebellar PCs in transgenic mice is not sufficient to cause progressive motor impairment (Yvert et al., 2000). Indeed, ataxia and PC degeneration can develop in SCA7 mice in which mutant ataxin-7 is expressed throughout the brain, but not in PCs (Garden et al., 2002), indicating the importance of non-cell-autonomous degeneration in SCA7. To test whether excising mutant ataxin-7 in PCs would significantly alter the disease phenotype, we crossed *PrP-floxed-SCA7-92Q BAC* mice with a Purkinje cell protein 2 (Pcp2)-Cre line, obtained from the Jackson Laboratory (Barski et al., 2000). When we assessed the excision rate in *Pcp2-Cre;PrP-floxed-SCA7-92Q BAC* bigenic mice by immunofluorescent labeling with antibodies to EGFP and calbindin, we noted that 52% of all calbindin-positive PCs were also EGFP positive (Fig. 3A,B). Importantly, in the course of performing this analysis, we docu-
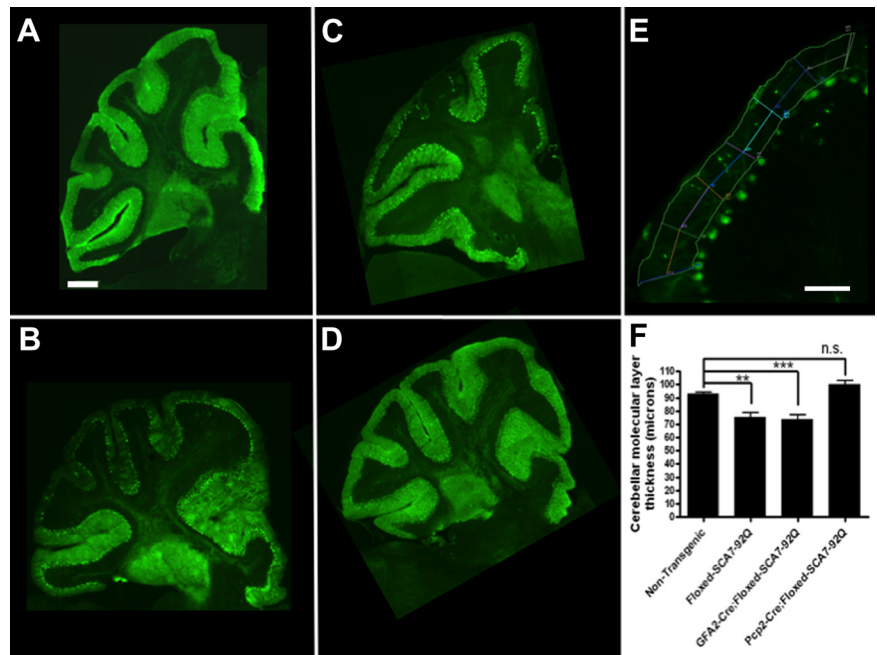
PrP-floxed-SCA7-92Q BAC mice (Fig. 4*C*); however, *Pcp2-Cre;PrP-floxed-SCA7-92Q BAC* cerebellar sections resembled cerebellar sections from nontransgenic controls (Fig. 4*A–D*).

To further investigate the effect of conditional ataxin-7 excision from selected cell populations in the cerebellum, we quantified molecular layer thickness in dorsal cerebellum. When we measured the width of the molecular layer along the outside of each folium from the pial surface to the PC layer boundary at 100 μm intervals (Fig. 4*E*), we found that molecular layer thickness was significantly reduced from an average of 92.8 μm in nontransgenic controls to 75.5 μm in *PrP-floxed-SCA7-92Q BAC* mice (Fig. 4*F*). Although *Gfa2-Cre;PrP-floxed-SCA7-92Q BAC* mice had a similarly reduced molecular layer thickness, *Pcp2-Cre;PrP-floxed-SCA7-92Q BAC* bigenic mice exhibited molecular layer thickness values that were comparable to nontransgenic controls and markedly increased versus *PrP-floxed-SCA7–92Q BAC* mice (Fig. 4*F*). The molecular layer thickness in *Gfa2-Cre* and *Pcp2-Cre* singly transgenic mice did not differ from nontransgenic animals (data not shown). These findings indicate that excision of mutant ataxin-7 from PCs and IO neurons rescues PC neurodegeneration in SCA7 transgenic mice, while excision of mutant ataxin-7 from BG does not prevent such PC pathology.

Figure 4. Excision of polyQ-ataxin-7 from Purkinje cells and inferior olive prevents cerebellar degeneration in *PrP-floxed-SCA7-92Q BAC* mice. *A–D*, Anti-calbindin antibody staining of cerebellar sections. Calbindin immunoreactivity in nontransgenic control cerebellum is intense (*A*), in contrast to the marked loss of calbindin immunoreactivity in the dorsal cerebellar folia of *PrP-floxed-SCA7-92Q BAC* mice (*B*); *Gfa2-Cre;PrP-floxed-SCA7-92Q BAC* mice (*C*) also display reduced calbindin immunoreactivity and molecular layer thinning, but cerebellar sections from *Pcp2-Cre;PrP-floxed-SCA7-92Q BAC* mice (*D*) exhibit intense calbindin staining comparable to nontransgenic controls. *E*, We quantified cerebellar molecular layer thickness by taking measurements at 100 μm intervals (perpendicular lines) along the outer region of three dorsal cerebellar folia per section. *F*, Results of cerebellar molecular layer quantifications ($n = 6 –7$/group). *PrP-floxed-SCA7-92Q BAC* and *Gfa2-Cre;PrP-floxed-SCA7-92Q BAC* animals have significantly thinner molecular layers in their dorsal cerebellar folia (**$p < 0.01$ and ***$p < 0.001$, respectively, one-way ANOVA with Bonferroni's *post hoc* test). Cerebellar molecular layer thickness of *Pcp2-Cre;PrP-floxed-SCA7-92Q BAC* animals, however, was unchanged from nontransgenic controls. Error bars indicate SEM. Scale bars: *A*, 300 μm; *E*, 100 μm.

PolyQ-ataxin-7 excision in Purkinje cells and inferior olive, but not in Bergmann glia, prevents Bergmann glia degeneration

As BG exhibit morphological pathology and dysfunction in SCA7 (Garden et al., 2002; Custer et al., 2006), we examined BG morphology in *PrP-floxed-SCA7-92Q BAC* mice and the two bigenic lines. After staining sagittal cerebellar sections for GFAP to visualize BG processes, we generated 3-D images of dorsal cerebellar folia, deconvolved them, and transformed them into 2-D images by creating brightest-point projections. This analysis revealed that *PrP-floxed-SCA7-92Q BAC* mice have remarkably fewer BG processes in the cerebellar molecular layer (Fig. 5*A,B*). Although the morphology of BG in *Gfa2-Cre;PrP-floxed-SCA7-92Q BAC* bigenic mice resembled that of *PrP-floxed-SCA7-92Q BAC* mice, BG in *Pcp2-Cre;PrP-floxed-SCA7-92Q BAC* mice exhibited more prominent processes, indicative of an intermediate pathology between nontransgenic controls and *PrP-floxed-SCA7-92Q BAC* mice (Fig. 5*A–D*). To quantify BG pathology, we counted the number of GFAP-positive BG processes that crossed a 150 μm line drawn parallel to, and 50 μm from, the pial surface (Fig. 5*E*). *PrP-floxed-SCA7-92Q BAC* mice harbored significantly fewer BG processes than nontransgenic controls (Fig. 5*F*). Surprisingly, BG processes were also markedly reduced in *Gfa2-Cre;PrP-floxed-SCA7-92Q BAC* mice, similar to *PrP-floxed-SCA7-92Q BAC* mice. BG process number in *Pcp2-Cre;PrP-floxed-SCA7-92Q BAC* bigenic mice was not significantly different from nontransgenic mice or from *PrP-floxed-SCA7-92Q BAC* mice, indicative

of an intermediate phenotype (Fig. 5*F*). Neither *Gfa2-Cre* nor *Pcp2-Cre* singly transgenic mice differed from nontransgenic controls (data not shown). Hence, excision of mutant ataxin-7 from PCs and IO neurons ameliorated BG histopathology, while elimination of mutant ataxin-7 expression from BG did not improve BG degeneration. This finding represents the first demonstration that BG dysfunction and degeneration in SCA7 is non-cell autonomous.

PolyQ-ataxin-7 excision from Bergmann glia, Purkinje cells, and inferior olive delays SCA7 disease onset

Because excising polyQ-ataxin-7 from BG, or from PCs and IO neurons, partially rescued SCA7 neurodegeneration, we proceeded to test whether eliminating mutant ataxin-7 from all three cell types would further ameliorate SCA7 disease pathogenesis. To do so, we generated triple transgenic mice that carried the *PrP-floxed-SCA7-92Q* BAC, the *Pcp2-Cre* transgene, and the *Gfa2-Cre* transgene. Composite phenotype analysis revealed that such triple transgenic mice exhibit very late disease onset, but, once manifested, neurological abnormalities are progressive (Fig. 6*A*). Rotarod analysis, however, indicated that triple transgenic mice retain normal motor coordination function and perform dramatically better than singly transgenic *PrP-floxed-SCA7-92Q BAC* mice at 40 weeks of age (Fig. 6*B*).

To quantify the delay in onset, we pooled data from all *PrP-floxed-SCA7-92Q BAC*, nontransgenic, *Gfa2-Cre;PrP-floxed-SCA7-92Q BAC*, *Pcp2-Cre;PrP-floxed-SCA7-92Q BAC*, and triple transgenic mice analyzed during the course of this study.
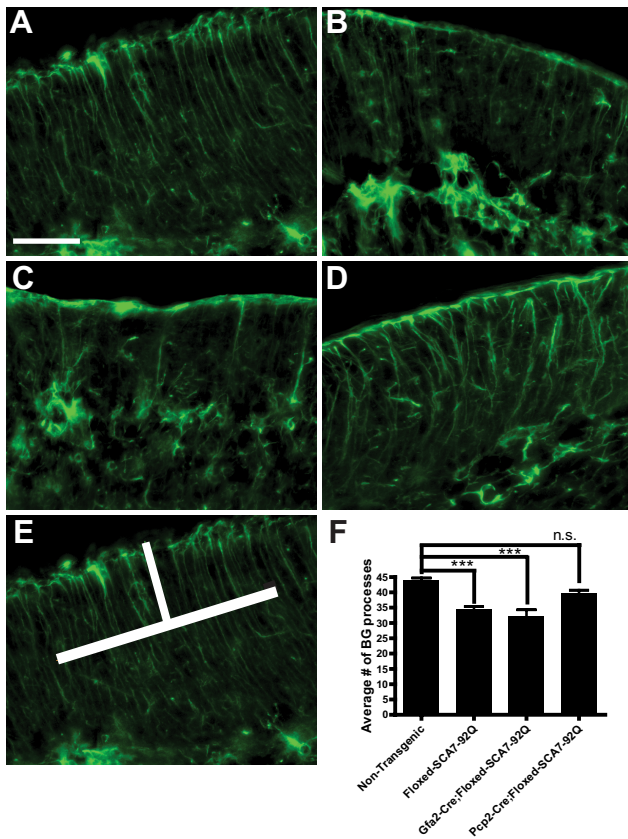
Figure 5. Excision of polyQ-ataxin-7 from Purkinje cells and inferior olive, but not Bergmann glia, prevents loss of glial processes. *A–D*, Anti-GFAP antibody staining of dorsal cerebellar folia. Comparison of nontransgenic controls (*A*) to *PrP-floxed-SCA7-92Q BAC* mice (*B*) demonstrates an obvious reduction in Bergmann glia processes in the *PrP-floxed-SCA7-92Q BAC* mice; *Gfa2-Cre;PrP-floxed-SCA7-92Q BAC* cerebellar sections (*C*) resembled *PrP-floxed-SCA7-92Q BAC* sections, while *Pcp2-Cre;PrP-floxed-SCA7-92Q BAC* cerebellar sections (*D*) appeared comparable to nontransgenic controls. *E*, We quantified Bergmann glia processes by counting the number of GFAP-positive processes that cross a 150 μm line drawn parallel to, and ~50 μm from, the pial surface. *F*, Results of quantifications of Bergmann glia processes (*n* = 6/group). *PrP-floxed-SCA7-92Q BAC* and *Gfa2-Cre;PrP-floxed-SCA7-92Q* BAC animals have significantly fewer Bergmann glia processes compared with nontransgenic mice (***p* < 0.001, one-way ANOVA with Bonferroni's *post hoc* test). However, the number of Bergmann glia processes in *Pcp2-Cre;PrP-floxed-SCA7-92Q BAC* mice is intermediate between nontransgenic controls and *PrP-floxed-SCA7-92Q BAC* mice. Error bars indicate SEM. Scale bar, 30 μm.

One-way ANOVA testing, followed by a Bonferroni's multiple-comparison *post hoc* analysis, was conducted for all composite phenotype data. This analysis showed that *PrP-floxed-SCA7-92Q BAC* mice display neurological abnormalities at 20 weeks of age (*p* < 0.001), establishing the age of onset. Both *Gfa2-Cre;PrP-floxed-SCA7-92Q BAC* and *Pcp2-Cre;PrP-floxed-SCA7-92Q BAC* bigenic mice exhibit significant neurological impairments by 25 weeks of age (*p* < 0.01 and *p* < 0.001, respectively). The triple transgenic mice, however, do not develop statistically significant neurological deficits until 40 weeks of age (*p* < 0.01), a delay of onset of 20 weeks. Thus, SCA7 mice, in which the ataxin-7 transgene is excised from BG, PCs, and IO neurons, exhibit a dramatically improved phenotype, underscoring the combined importance of all these components of the cerebellar circuitry.

To further assess the effect of removing mutant ataxin-7 expression from BG, PCs, and IO neurons, we analyzed the histological phenotype of the trigenic animals. Mean cerebellar
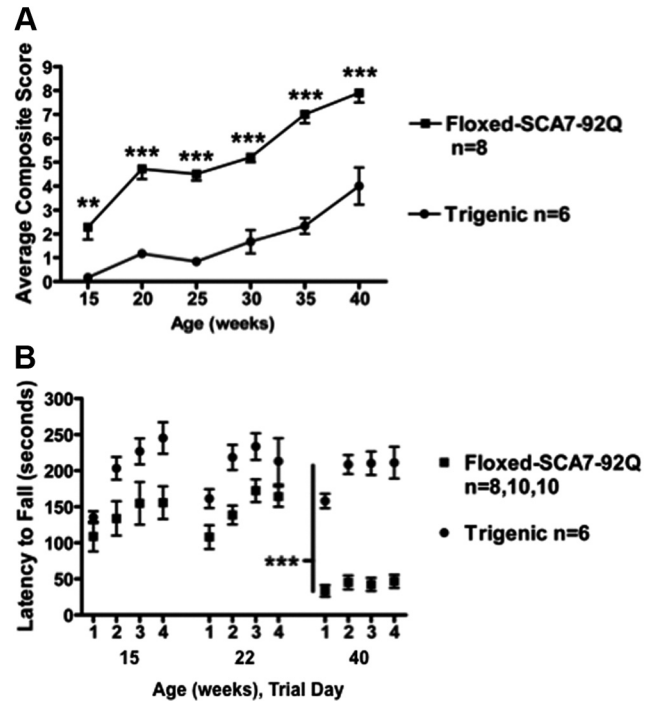
Figure 6. Excision of polyQ-ataxin-7 from Bergmann glia, Purkinje cells, and inferior olive greatly retards neurological disease onset in *PrP-floxed-SCA7-92Q BAC* mice. *A*, Composite phenotype scoring of *Gfa2-Cre;Pcp2-Cre;PrP-floxed-SCA7-92Q BAC* (trigenic) mice reveals markedly delayed onset of a progressive behavioral phenotype, and superior performance scores compared with *PrP-floxed-SCA7-92Q BAC* mice at all time points tested (***p* < 0.01, ****p* < 0.001, two-way ANOVA with Bonferroni's *post hoc* test; *n* = 6–8/group). Error bars indicate SEM. *B*, Trigenic mice consistently performed better on the accelerating rotarod than *PrP-floxed-SCA7-92Q BAC* mice at all time points; and rotarod performance was dramatically superior at 40 weeks of age (****p* < 0.001, two-way ANOVA with Bonferroni's *post hoc* test; *n* = 6–10/group). Error bars indicate SEM.

molecular layer thickness of the triple transgenic mice (100.2 μm) did not significantly differ from that measured in the *Pcp2-Cre;PrP-floxed-SCA7-92Q* bigenic mice (100.0 μm). To address the possibility that mutant ataxin-7-mediated degeneration of cerebellar granule cell neurons could contribute to the SCA7 phenotype, we analyzed the cerebellar granule cell layer in nontransgenic and *PrP-floxed-SCA7-92Q BAC* mice. No overt morphological changes were noted, and the width of the granule layer was modestly increased in *PrP-floxed-SCA7-92Q BAC* mice compared with nontransgenic controls (data not shown). These results indicate that delay of disease onset until 40 weeks of age in *Gfa2-Cre;Pcp2-Cre; PrP-floxed-SCA7-92Q BAC* transgenic mice is best attributed to incomplete excision of ataxin-7 cDNA from PCs, IO neurons, and BG.

Discussion

In this study, we report a new SCA7 mouse model in which ataxin-7 gene expression can be controlled by Cre recombinase. In this model, a murine PrP BAC containing >50 kb of DNA 5′ to the PrP translational start site produced widespread expression of ataxin-7-92Q, including in PC neurons. In a prior study, a smaller PrP promoter fragment lacking key regulatory elements to drive broad expression of ataxin-7-92Q was used, but expression in PCs was not observed (Garden et al., 2002). *PrP-floxed-SCA7-92Q BAC* mice developed progressive ataxia and cerebellar degeneration typical of other SCA7 models (Garden et al., 2002; Yoo et al., 2003; Custer et al., 2006; Wang et al., 2010). When *PrP-floxed-SCA7-92Q BAC* mice were crossed with mice with

ubiquitous Cre expression, mutant ataxin-7 was no longer produced and no behavioral phenotype developed, validating the loxP sites. Excision of ataxin-7-92Q from BG in the cerebella of *Gfa2-Cre;PrP-floxed-SCA7-92Q BAC* bigenic mice significantly ameliorated neurological abnormalities measured by composite phenotype scoring (Guyenet et al., 2010), but did not prevent cerebellar molecular layer thinning or BG process loss. Excision of ataxin-7-92Q from PCs and IO neurons improved motor behavior and protected against cerebellar molecular layer thinning and BG process loss. These findings indicate that expression of mutant ataxin-7 in BG is not required for glial degeneration. However, expression of mutant ataxin-7 in PCs and IO neurons contributes to BG pathology. Thus, SCA7 exhibits non-cell-autonomous BG degeneration, revealing for the first time that neuronal health directly impacts BG in SCA7.

Studies over the last decade support the realization that the cellular basis of neurodegenerative disorders is not simply cell autonomous. An important example comes from a series of studies on familial amyotrophic lateral sclerosis (ALS) due to dominant, gain-of-function mutations in superoxide dismutase 1 (SOD1). This form of ALS has been extensively studied since its genetic basis was defined in 1993 (Rosen et al., 1993). Transgenic expression of disease-causing SOD1 mutations in mice recapitulated key features of human ALS motor neuron degeneration (Gurney et al., 1994). These early mouse models used the native SOD1 promoter, resulting in ubiquitous expression of the mutant SOD1 protein. When transgenic strategies relying upon neuron-restricted expression of mutant SOD1 failed to produce significant motor neuron disease in mice (Pramatarova et al., 2001; Lino et al., 2002), many groups theorized that motor neuron degeneration might be non-cell autonomous in this form of ALS. Production of chimeric mice containing different mixtures of normal and mutant-expressing SOD1 cells allowed investigators to definitively show that motor neuron expression of mutant SOD1 is not sufficient for disease (Clement et al., 2003). Instead, non-neuronal cells must express mutant SOD1 for neighboring motor neurons to degenerate. Current models of ALS postulate that a variety of different molecular pathologies contribute to the motor neuron degeneration by eliciting damage within different cell types, and that death of the motor neuron does not occur in isolation from its connected glial, vascular, and immune system partners (Ilieva et al., 2009).

In SCA7, it is also clear that neurodegeneration is not simply cell autonomous. Our study examined the roles of BG, PCs, and IO neurons, and found that all of these cell types contribute to SCA7 PC degeneration. We previously reported that expression of mutant ataxin-7 in BG in *Gfa2-SCA7–92Q* transgenic mice is sufficient to cause PC degeneration (Custer et al., 2006). In the current study, removal of ataxin-7-92Q from PCs and IO neurons prevented PC degeneration (as measured by cerebellar molecular layer thinning), despite continued expression of mutant ataxin-7 protein in BG. One likely explanation for the difference between these two studies is that *PrP-floxed-SCA7-92Q BAC* mice express mutant ataxin-7 at levels less than that of the endogenous gene, while expression in *Gfa2-SCA7–92Q* transgenic mice exceeded endogenous levels. Furthermore, isolated expression of mutant ataxin-7 in BG resulted in late-onset ataxia and PC degeneration in the *Gfa2-SCA7–92Q* model. When mutant ataxin-7 is expressed ubiquitously at lower levels, reduction of mutant ataxin-7 expression in PCs and IO neurons is more beneficial than excision of mutant ataxin-7 in BG. Thus, expression of mutant ataxin-7 in IO neurons, in combination with expression in
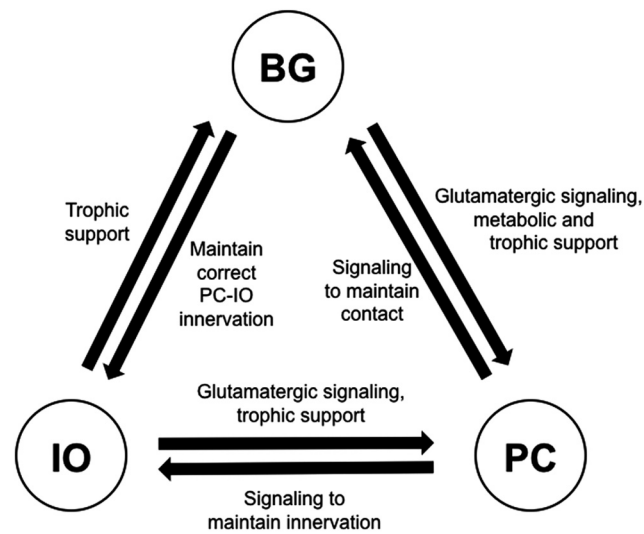
Figure 7. Interdependent connections between BG, PC, and IO account for the multi-cell type origin of SCA7 neurodegeneration. BG, PCs, and IO neurons each engage in bilateral interactions to yield an interdependent neural–glial network in which the function and survival of all cell types are assured together. During SCA7 disease pathogenesis, dysfunction of one cell type will inevitably impact the other connected cell types due to loss of trophic support and/or release of excitotoxic or inflammatory mediators. Altered function in one cell type thus culminates in all cell types failing to maintain appropriate signaling or other key functions, thereby exacerbating damage in the initial cell type while propagating abnormalities in the other connected cell types.

PCs, produces greater cerebellar toxicity than mutant ataxin-7 expression in BG. Nonetheless, our current findings continue to support an important role for BG in SCA7 pathogenesis. Excision of the disease gene from BG alone does ameliorate the disease phenotype, and excision of mutant ataxin-7 from BG in combination with PCs and IO neurons yields a synergistic effect on the delay of symptom onset.

An important and unexpected observation in this study is that a well established *Pcp2-Cre* transgenic driver line (Barski et al., 2000) expresses Cre-recombinase in both PCs and IO neurons. This permitted us to evaluate the contribution of IO neurons and PCs to cerebellar degeneration in SCA7, but prevented us from delineating the individual role of each cell type in SCA7 pathogenesis. Previous studies in transgenic mice have shown that polyQ-ataxin-7 expression restricted to PCs produces a very mild, late-onset phenotype (Yvert et al., 2000). However, expression in other cerebellar cell types, but not in PCs, yields more severe SCA7 disease (Garden et al., 2002; Custer et al., 2006). Together, these studies, in conjunction with data presented here, suggest that IO neuron dysfunction is a major contributor to SCA7 disease pathogenesis. A principal role for IO neurodegeneration in SCA7 is suggested not only by our findings, but also by work done independently on a different SCA7 transgenic mouse model (Wang et al., 2010).

How might IO neuron dysfunction result in cerebellar degeneration in SCA7? One function of IO neurons is to deliver IGF-1, an important survival factor for PCs, to the cerebellar molecular layer (Nieto-Bona et al., 1993). Exogenous IGF-1 ameliorates PC degeneration (Tolbert and Clark, 2003; Carrascosa et al., 2004) and promotes glial glutamate transporter gene expression in BG (Gamboa and Ortega, 2002). Impaired GLAST transcription has been documented in SCA7 transgenic mice (Custer et al., 2006), thus loss of IGF-1 delivery from IO neuron CFs may contribute to reduced GLAST gene expression in SCA7. Loss of CFs may also

explain the observation that the GluRδ2 AMPA receptor subunit is upregulated in cerebellar lysates from ataxin-7–52Q transgenic mice (Chou et al., 2010). GluRδ2 is found exclusively at PC–parallel fiber (PC-PF) synapses (Kurihara et al., 1997). Deletion of GluRδ2 in mice causes reduced PC–PF synapses and abnormal extra PC–CF synapses (Kashiwabuchi et al., 1995). It is possible that loss of CF input due to cell-autonomous degeneration of IO neurons leads to increased PC–PF synapses and thus increased GluRδ2 expression (Chou et al., 2010). Another explanation might involve transcriptional dysregulation resulting in increased GluRδ2 expression, increased PC–PF synapses, and subsequent reduction of PC–CF synapses, contributing to degeneration of IO neurons. BG are a component of both the PC–PF and PC–CF tripartite synapse; thus, disruption of inputs to PCs may in turn cause BG dysfunction and/or degeneration. Because mutant ataxin-7 disrupts normal gene transcription (McMahon et al., 2005; Palhan et al., 2005; Helmlinger et al., 2006), it is also possible that the molecular pathways involved in maintaining appropriate connections between PCs, IO neurons, and BG are altered by transcriptional dysregulation in a cell type-specific fashion. It will be critical to identify the cellular processes that mutant ataxin-7 disturbs within each cell type, and how these abnormalities lead to disruptions in the PC–IO neuron–BG network (Fig. 7).

Triple transgenic mice harboring the *PrP-floxed-SCA7-92Q BAC*, *Gfa2-Cre*, and *Pcp2-Cre* transgenes exhibited a dramatic rescue from neurological disease and PC degeneration. Remarkably, removing mutant ataxin-7 from these cell populations delayed disease onset by 20 weeks (i.e., twofold). Although disease pathology in the triple transgenic mice could stem from expression of mutant ataxin-7 in cerebellar GCNs, we carefully evaluated GCN morphology, but did not observe any GCN abnormalities, suggesting instead that incomplete excision of mutant ataxin-7 expression from PCs, IO neurons, and BG likely accounts for the ultimate development of a disease phenotype in these mice. Our results demonstrate that PCs, IO neurons, and BG are all involved in SCA7 disease pathogenesis (Fig. 7). PolyQ-ataxin-7 consequently leads to dysfunction in each of these different cell types, preventing them from performing key functions or maintaining healthy connections with their interdependent neighbors. Cerebellar neurodegeneration in SCA7 may thus be viewed as a coincident set of pathological alterations that occur within a highly interconnected network composed of neurons and glia. Our findings underscore the complexity of SCA7 disease pathogenesis and suggest that reversing toxicity in a single cell type is unlikely to reverse the course of disease. However, these findings suggest that effective gene-silencing strategies delivered to any involved cell type should yield significant benefit to afflicted patients.

References

Barski JJ, Dethleffsen K, Meyer M (2000) Cre recombinase expression in cerebellar Purkinje cells. Genesis 28:93–98.

Besnard F, Brenner M, Nakatani Y, Chao R, Purohit HJ, Freese E (1991) Multiple interacting sites regulate astrocyte-specific transcription of the human gene for glial fibrillary acidic protein. J Biol Chem 266:18877–18883.

Carrascosa C, Torres-Aleman I, Lopez-Lopez C, Carro E, Espejo L, Torrado S, Torrado JJ (2004) Microspheres containing insulin-like growth factor I for treatment of chronic neurodegeneration. Biomaterials 25:707–714.

Chou AH, Chen CY, Chen SY, Chen WJ, Chen YL, Weng YS, Wang HL (2010) Polyglutamine-expanded ataxin-7 causes cerebellar dysfunction by inducing transcriptional dysregulation. Neurochem Int 56:329–339.

Clement AM, Nguyen MD, Roberts EA, Garcia ML, Boillée S, Rule M, McMahon AP, Doucette W, Siwek D, Ferrante RJ, Brown RH Jr, Julien JP,

Goldstein LS, Cleveland DW (2003) Wild-type nonneuronal cells extend survival of SOD1 mutant motor neurons in ALS mice. Science 302:113–117.

Custer SK, Garden GA, Gill N, Rueb U, Libby RT, Schultz C, Guyenet SJ, Deller T, Westrum LE, Sopher BL, La Spada AR (2006) Bergmann glia expression of polyglutamine-expanded ataxin-7 produces neurodegeneration by impairing glutamate transport. Nat Neurosci 9:1302–1311.

Gamboa C, Ortega A (2002) Insulin-like growth factor-1 increases activity and surface levels of the GLAST subtype of glutamate transporter. Neurochem Int 40:397–403.

Garden GA, La Spada AR (2008) Molecular pathogenesis and cellular pathology of spinocerebellar ataxia type 7 neurodegeneration. Cerebellum 7:138–149.

Garden GA, Libby RT, Fu YH, Kinoshita Y, Huang J, Possin DE, Smith AC, Martinez RA, Fine GC, Grote SK, Ware CB, Einum DD, Morrison RS, Ptacek LJ, Sopher BL, La Spada AR (2002) Polyglutamine-expanded ataxin-7 promotes non-cell-autonomous Purkinje cell degeneration and displays proteolytic cleavage in ataxic transgenic mice. J Neurosci 22:4897–4905.

Gurney ME, Pu H, Chiu AY, Dal Canto MC, Polchow CY, Alexander DD, Caliendo J, Hentati A, Kwon YW, Deng HX (1994) Motor neuron degeneration in mice that express a human Cu,Zn superoxide dismutase mutation. Science 264:1772–1775.

Guyenet SJ, Furrer SA, Damian VM, Baughan TD, La Spada AR, Garden GA (2010) A simple composite phenotype scoring system for evaluating mouse models of cerebellar ataxia. J Vis Exp pii:1787.

Helmlinger D, Hardy S, Abou-Sleymane G, Eberlin A, Bowman AB, Gansmüller A, Picaud S, Zoghbi HY, Trottier Y, Tora L, Devys D (2006) Glutamine-expanded ataxin-7 alters TFTC/STAGA recruitment and chromatin structure leading to photoreceptor dysfunction. PLoS Biol 4:e67.

Huang H, Bordey A (2004) Glial glutamate transporters limit spillover activation of presynaptic NMDA receptors and influence synaptic inhibition of Purkinje neurons. J Neurosci 24:5659–5669.

Ilieva H, Polymenidou M, Cleveland DW (2009) Non-cell autonomous toxicity in neurodegenerative disorders: ALS and beyond. J Cell Biol 187:761–772.

Kashiwabuchi N, Ikeda K, Araki K, Hirano T, Shibuki K, Takayama C, Inoue Y, Kutsuwada T, Yagi T, Kang Y (1995) Impairment of motor coordination, Purkinje cell synapse formation, and cerebellar long-term depression in GluRδ2 mutant mice. Cell 81:245–252.

Kurihara H, Hashimoto K, Kano M, Takayama C, Sakimura K, Mishina M, Inoue Y, Watanabe M (1997) Impaired parallel fiber—Purkinje cell synapse stabilization during cerebellar development of mutant mice lacking the glutamate receptor δ2 subunit. J Neurosci 17:9613–9623.

La Spada AR, Fu YH, Sopher BL, Libby RT, Wang X, Li LY, Einum DD, Huang J, Possin DE, Smith AC, Martinez RA, Koszdin KL, Treuting PM, Ware CB, Hurley JB, Ptácek LJ, Chen S (2001) Polyglutamine-expanded ataxin-7 antagonizes CRX function and induces cone-rod dystrophy in a mouse model of SCA7. Neuron 31:913–927.

Lino MM, Schneider C, Caroni P (2002) Accumulation of SOD1 mutants in postnatal motoneurons does not cause motoneuron pathology or motoneuron disease. J Neurosci 22:4825–4832.

McMahon SJ, Pray-Grant MG, Schieltz D, Yates JR 3rd, Grant PA (2005) Polyglutamine-expanded spinocerebellar ataxia-7 protein disrupts normal SAGA and SLIK histone acetyltransferase activity. Proc Natl Acad Sci U S A 102:8478–8482.

Mount HT, Dean DO, Alberch J, Dreyfus CF, Black IB (1995) Glial cell line-derived neurotrophic factor promotes the survival and morphologic differentiation of Purkinje cells. Proc Natl Acad Sci U S A 92:9092–9096.

Nieto-Bona MP, Garcia-Segura LM, Torres-Aleman I (1993) Orthograde transport and release of insulin-like growth factor I from the inferior olive to the cerebellum. J Neurosci Res 36:520–527.

Novak A, Guo C, Yang W, Nagy A, Lobe CG (2000) Z/EG, a double reporter mouse line that expresses enhanced green fluorescent protein upon Cre-mediated excision. Genesis 28:147–155.

Palhan VB, Chen S, Peng GH, Tjernberg A, Gamper AM, Fan Y, Chait BT, La Spada AR, Roeder RG (2005) Polyglutamine-expanded ataxin-7 inhibits STAGA histone acetyltransferase activity to produce retinal degeneration. Proc Natl Acad Sci U S A 102:8472–8477.

Pramatarova A, Laganière J, Roussel J, Brisebois K, Rouleau GA (2001) Neuron-specific expression of mutant superoxide dismutase 1 in

transgenic mice does not lead to motor impairment. J Neurosci 21:3369–3374.

Rosen DR, Siddique T, Patterson D, Figlewicz DA, Sapp P, Hentati A, Donaldson D, Goto J, O'Regan JP, Deng HX (1993) Mutations in Cu/Zn superoxide dismutase gene are associated with familial amyotrophic lateral sclerosis. Nature 362:59–62.

Tolbert DL, Clark BR (2003) GDNF and IGF-1 trophic factors delay hereditary Purkinje cell degeneration and the progression of gait ataxia. Exp Neurol 183:205–219.

Wang HL, Chou AH, Lin AC, Chen SY, Weng YH, Yeh TH (2010) Polyglutamine-expanded ataxin-7 upregulates Bax expression by activating p53 in cerebellar and inferior olivary neurons. Exp Neurol 224:486–494.

Yoo SY, Pennesi ME, Weeber EJ, Xu B, Atkinson R, Chen S, Armstrong DL, Wu SM, Sweatt JD, Zoghbi HY (2003) SCA7 knockin mice model human SCA7 and reveal gradual accumulation of mutant ataxin-7 in neurons and abnormalities in short-term plasticity. Neuron 37:383–401.

Yvert G, Lindenberg KS, Picaud S, Landwehrmeyer GB, Sahel JA, Mandel JL (2000) Expanded polyglutamines induce neurodegeneration and trans-neuronal alterations in cerebellum and retina of SCA7 transgenic mice. Hum Mol Genet 9:2491–2506.

Zhuo L, Theis M, Alvarez-Maya I, Brenner M, Willecke K, Messing A (2001) hGFAP-cre transgenic mice for manipulation of glial and neuronal function in vivo. Genesis 31:85–94.